ACS APPLIED MATERIALS & INTERFACES

Research Article

www.acsami.org

Chimeric Nanoparticle: A Platform for Simultaneous Targeting of Phosphatidylinositol-3-Kinase Signaling and Damaging DNA in Cancer Cells

Sandeep Palvai,[†] Piyush More,[†] Nikunj Mapara, and Sudipta Basu*

Department of Chemistry, Indian Institute of Science Education and Research (IISER)-Pune, Pune, 411008, Maharashtra, India

Supporting Information

ABSTRACT: Phosphatidylinositol-3-kinase (PI3K) signaling has been hijacked in different types of cancers. Hence, PI3K inhibitors have emerged as novel targeted therapeutics in cancer treatment as mono and combination therapy along with other DNA damaging drugs. However, targeting PI3K signaling with small molecules leads to the emergence of drug resistance and severe side effects to the cancer patients. To address these, we have developed a biocompatible, biodegradable cholesterol-based chimeric nanoparticle (CNP), which can simultaneously load PI103, doxorubicin, and cisplatin in a controlled ratiometric manner. Size, shape, and morphology of these CNPs were characterized by dynamic light scattering (DLS), field-emission scanning electron microscopy (FESEM), atomic force microscopy (AFM), and transmission electron microscopy (TEM). Increased amounts of PI103, doxorubicin, and cisplatin were released from CNPs through controlled and continuous manner over 120 h at pH = 5.5 compared to neutral pH. The CNPs showed much enhanced *in vitro* cytotoxicity in HeLa, HL60, MCF7, and MDA-MB-231 cancer cells compared to a free drug cocktail at 24 and 48 h by inducing apoptosis. Confocal laser scanning microscopy (CLSM) imaging revealed that indeed these CNPs were internalized into subcellular lysosomes through endocytosis in a time dependent mode over 6 h and retained inside for 48 h in HeLa, MDA-MB-231, and MCF7 cells. These CNPs showed their efficacy by damaging DNA and inhibiting Akt as a downstream modulator of PI3K signaling in HeLa cervical cancer cells. These CNPs have the potential to open up new directions in next-generation nanomedicine by simultaneous targeting of multiple oncogenic signaling pathways and inducing DNA damage for augmented therapeutic outcome by reducing toxic side effects and overcoming drug resistance.

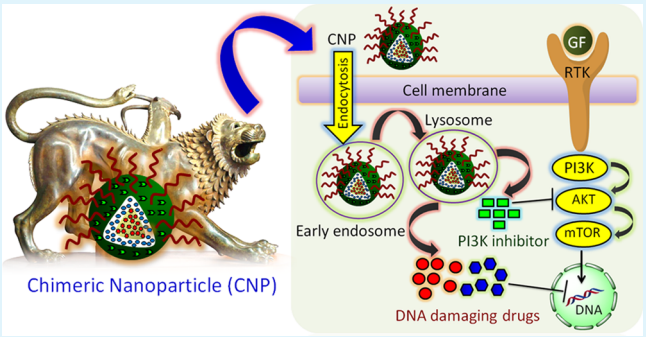

KEYWORDS: *chimeric nanoparticle, PI3K signaling, DNA damage, doxorubicin, cisplatin, PI103, cancer*

1. INTRODUCTION

Cancer has evolved as the second most devastating disease globally.[1,2] Despite having tremendous advancement in cancer chemotherapeutic treatments, the majority of tumors can escape monotherapy by emergence of intrinsic or acquired resistance mechanisms.[3,4] In the past two decades, the phosphatidylinositol-3-kinase (PI3K) family has emerged as one of the most important targets in cancer therapy due to its myriad functions to integrate signals from various environmental cues for altering multiple intracellular signaling for controlling cell growth, proliferation, survival, motility, and metastasis.[5−7] Consequently, significant effort was devoted to develop small molecule PI3K inhibitors for cancer therapy.[8−10] However, PI3K signaling plays critical functions in controlling insulin metabolism and glucose homeostasis,[11−13] leading to dose-dependent hyperglycemia among PI3K-inhibitor treated patients.[14] Moreover, survival of cancer cells under stressful conditions by upregulating PI3K signaling prompted the need for a combination strategy with DNA damaging drugs to enhance therapeutic efficacy in cancer treatment.[10] Recently, several studies showed the synergistic effects of combining PI3K inhibitors with cytotoxic drugs in treating different types of cancers.[15−17] Although, these combination strategies indicated improved therapeutic outcomes, the drug cocktails can diffuse unsystematically throughout the entire body to escalate severe toxic side effects and poor accumulation into tumor tissue for optimal effects. Nanocarriers have revolutionized cancer theranostics in the past couple of decades due to their capability to increase drug solubility, extend drug stability in blood circulation, reduce off-target adverse effects, and accumulate drugs in the tumor tissues.[18−21] Nanocarriers having a size <300 nm can accumulate specifically into the tumor due to unique permeable tortuous angiogenic blood vessels.[22−24] Several nanocarriers including liposome,[25,26]

Received: May 9, 2015
Accepted: August 10, 2015
Published: August 10, 2015

DOI: 10.1021/acsami.5b04015
ACS Appl. Mater. Interfaces 2015, 7, 18327−18335

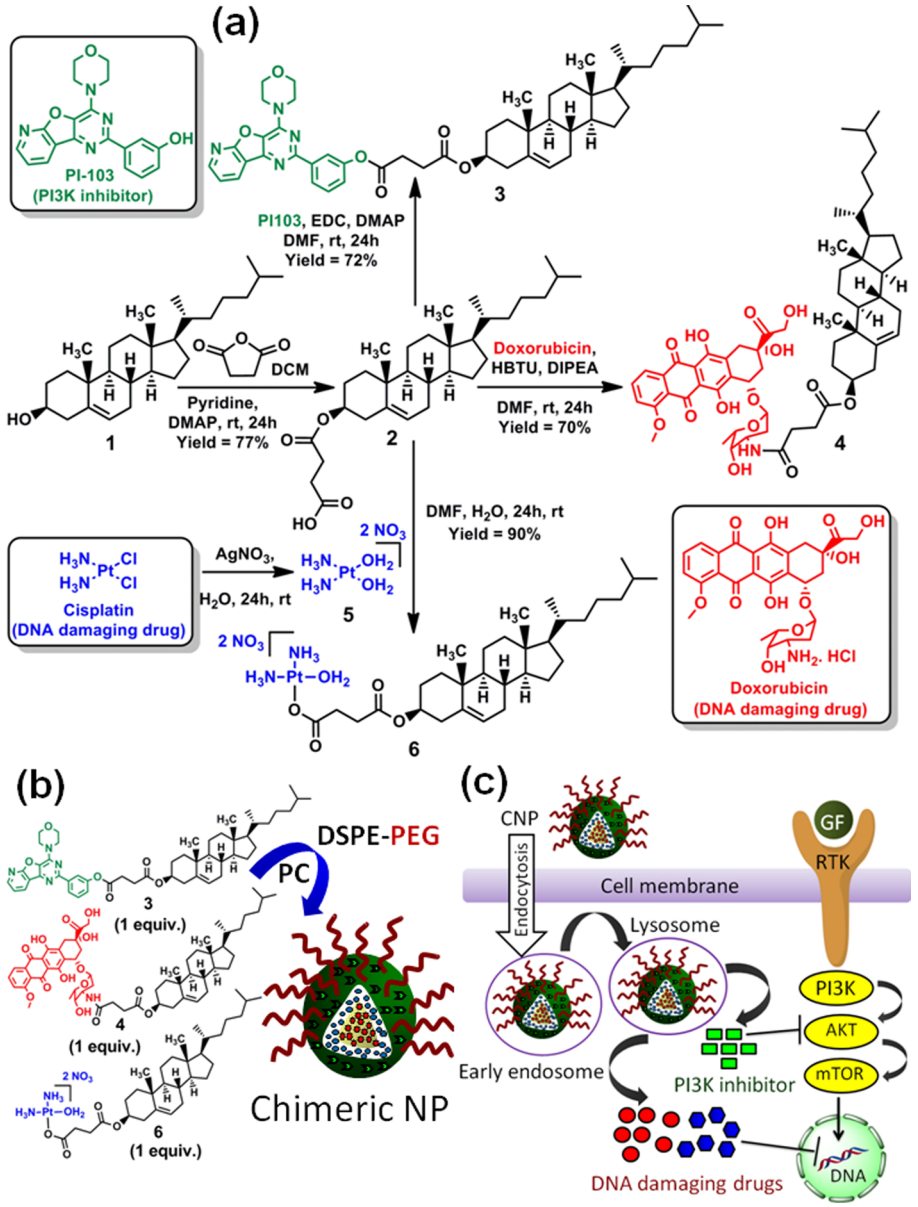

Figure 1. Schematic diagram of engineering chimeric nanoparticles (CNPs) and cellular internalization. (a) Synthesis of cholesterol−drug conjugates. (b) Schematic representation of CNP synthesis. (c) Hypothesized internalization of CNPs into cancer cells through lysosomes to target PI3K signaling and damage DNA.

polymeric nanoparticles,[27−29] dendrimers,[30,31] graphene oxide,[32,33] carbon nanotubes,[34] mesoporous silica nanospheres,[35] nanocells,[36] gel-liposomes,[37] layer-by-layer nanoparticles,[38] and minicells[39] have been developed to codeliver multiple drugs in combination with siRNA, DNA, and therapeutic proteins. Despite having a huge contribution of nanoplatforms in dual drug delivery in cancer therapeutics, not many attempts have been explored in delivering PI3K signaling inhibitors specifically into the tumor to reduce their off-target effects in healthy tissues as well as overcoming PI3K inhibitor related resistance.[40] To address this, recently, we have developed supramolecular lipidic nanoparticles to successfully target phosphatidylinositol-3-kinase signaling to overcome insulin resistance.[41] Moreover, a recent report revealed that sequential administration of PI3K inhibitors (PI103 and PI828) followed by cisplatin nanoparticles enhanced the antitumor efficacy in breast cancer.[42] However, there is no precedence of triple-drug combination therapy with PI103, doxorubicin, and cisplatin in a nanoparticle package to deliver in cancer. Inspired by the improved efficacy of PI3K inhibitors along with doxorubicin and cisplatin, we hypothesized that biocompatible, biodegradable, and versatile chimeric nanoparticles would accumulate inside the cancerous tissue by enhanced vascular permeabilization and internalize into the cancer cells by endocytosis for synchronized targeting of phosphatidylinositol-3-kinase signaling and inducing DNA damage for augmented therapeutic outcomes (Figure 1c). To this end, we engineered cholesterol based chimeric nanoparticles (CNPs) that can concurrently deploy PI103, doxorubicin, and cisplatin (Figure 1b). These CNPs permitted high triple drug loadings in a controlled ratiometric mode and demonstrated enhanced release in an acidic environment (mimics lysosomes in cancer cells) in a controlled and continuous manner over 120 h related to physiological pH =

DOI: 10.1021/acsami.5b04015
ACS Appl. Mater. Interfaces 2015, 7, 18327−18335

7.4. These CNPs exhibited improved cytotoxicity in different cancer cell lines compared to free drug combination at 24 and 48 h time points through induction of apoptosis. Moreover, these CNPs were internalized into the subcellular lysosomes in a time dependent manner over 6 h and remained inside the cells for 48 h. These CNPs induced cytotoxicity through apoptosis by damaging DNA, upregulating the DNA damage repair mechanism, and inhibiting PI3K signaling in HeLa cervical cancer cells. These CNPs showed their potential for simultaneous controlled loading and deployment of PI103 in rational amalgamation with doxorubicin and cisplatin inside the tumor cells for next-generation targeted cancer therapeutics.

2. MATERIALS AND METHODS

2.1. Material. All the chemicals, reagents, and solvents required for synthesis of cholesterol-drug conjugates and CNPs were purchased from Sigma-Aldrich. All the anticancer drugs were purchased from Selleck Chemicals. DSPE-PEG_{2000} and mini extruder were procured from Avanti Polar Lipids Inc. Cell culture media, LysoTracker DND-26, and *SlowFade* antifade reagents were bought from Life Technologies. Antiphospho-Akt (Thr308) rabbit monoclonal antibody was obtained from Merck Millipore.

2.2. Synthesis of Conjugate 2. Conjugate **2** was synthesized by following the procedure described in ref 41. Yield = 77%.

2.3. Synthesis of Cholesterol-PI103 Conjugate (3). Conjugate **3** was synthesized by following the procedure described in ref 41. Yield = 72%.

2.4. Synthesis of Cholesterol-Doxorubicin Conjugate (4). A mixture of compound **2** (5 mg, 0.01 mmol), HBTU (5.68 mg, 0.015 mmol), and DIPEA (2.5 μL, 0.015 mmol) in dry DMF (2 mL) was reacted for 10 min. Doxorubicin·HCl salt (6.9 mg, 0.012 mmol) was added and reacted for 24 h. To quench the reaction, 0.1 N HCl solution was added. The organic layer was washed with water (10 mL × 2). Then the collected organic solvent was dried and product was purified by silica gel column with dichloromethane/methanol as the eluent to afford a pure cholesterol-doxorubicin conjugate (**4**). Yield = 70%.

2.5. Synthesis of Aquated Cisplatin (5). Synthesis was carried out by following the method described in ref 43.

2.6. Synthesis of Cholesterol-Cisplatin Conjugate (6). Conjugate **6** was synthesized using the procedure in ref 43. Yield = 90%.

2.7. Synthesis of Chimeric Nanoparticles (CNPs). In short, 6.0 mg of PC 1 mg of each drug conjugate compound **3**, **4**, and **6**; and 0.6 mg of DSPE-PEG_{2000} were dissolved in DCM. Further CNPs were synthesized by the method described in ref 43. The dual drug loaded nanoparticles (CDDP-Dox-NP, Dox-PI103-NP and CDDP-PI103-NP) were synthesized using the same procedure from the corresponding cholesterol-drug conjugates in a 1:1 weight ratio.

2.8. Determination of Size, Shape, and Morphology of CNPs. Size, shape, and morphology of CNPs were determined by dynamic light scattering (DLS), field-emission scanning electron microscopy (FESEM), atomic force microscopy (AFM), and transmission electron microscopy (TEM). The sample preparation and measurements were done by the methods described in ref 44.

2.9. Stability of CNPs. Stability of the CNPs was performed by using the same procedure explained in ref 44.

2.10. Quantification of Drug Loading in CNPs. Loading of each drug in CNPs was quantified using the UV−vis spectroscopy method illustrated in refs 44 and 45.

2.11. Release of Triple Drugs from CNPs. The release of triple drugs in pH = 5.5 and pH = 7.4 was determined using the dialysis method described in refs 44 and 45.

2.12. *In Vitro* Assays. *In vitro* cell viability assays by MTT, apoptosis detection by the fluorescence activated cell sorting method (FACS), cellular internalization by confocal laser scanning microscopy (CLSM), and Western blot analysis were performed by the procedure described in our previous paper in ref 44.

3. RESULTS AND DISCUSSION

3.1. Development of Cholesterol−Drug Conjugates. We have chosen biocompatible and biodegradable cholesterol for developing the CNPs due to its ubiquitous nature as a cellular membrane component. The free hydroxyl group in cholesterol (**1**) was first converted to carboxylic acid by reacting with succinic anhydride, pyridine, and DMAP to achieve conjugate **2** in 77% yield (Figure 1a). We have chosen succinic acid as it is one of the major components in the tricarboxylic acid cycle (TCA) in mitochondria in our body.[46] We further reacted conjugate **2** with PI103 (PI3K inhibitor, currently in clinical study),[47,8] using EDC and DMAP as coupling reagents to afford a cholesterol-PI103 conjugate (**3**) in 72% yield. We also conjugated doxorubicin, a DNA binder and clinically approved anticancer agent, with conjugate **2** by amide linkage using HBTU/DIPEA to attain a cholesterol-doxorubicin conjugate (**4**) in 70% yield. Finally, cisplatin (CDDP), another DNA binding clinically approved drug, was converted to aquated *cis*-$Pt[(NH_3)_2(OH_2)_2]^{2+}$ (**5**),[48] which was further attached with conjugate **2** by a Pt−carboxylato bond[49] to synthesize a cholesterol−cisplatin conjugate (**6**) in 90% yield. The conjugates (**2**, **3**, **4**, and **6**) were characterized by ^{1}H, ^{13}C NMR, and HR-MS (Figures S1−S12 in the Supporting Information). Furthermore, conjugate **6** was characterized by ^{195}Pt NMR spectroscopy having peak at −1304 ppm (Figure S13 in the Supporting Information).[50]

3.2. Development of CNPs. We developed the CNPs from cholesterol−drug conjugates (**3**, **4**, and **6**), PC, and a DSPE-PEG_{2000} mixture in different ratios (Figure 1b).[43] We surface coated the CNPs with DSPE-PEG to provide a "stealth-like" property, evade the immune system, and improve long blood circulation half-life.[52] The drug loading in CNPs was quantified by UV−vis spectroscopy based on characteristic λ_{max} = 340 nm (PI103), 480 nm (doxorubicin), and 706 nm (cisplatin) from a standard absorbance versus concentration graph (Figure S14a−c in the Supporting Information). Due to rapid *in vivo* metabolism, it is necessary to achieve a nearly 10-fold increased concentration of PI103 for effective inhibition of PI3K and downstream Akt signaling.[53] Moreover, doxorubicin and cisplatin exert cardiotoxicity and nephrotoxicity, respectively.[54,55] Hence, it is highly important to package the drugs in optimal loading in the nanoplatform for combination therapy. To obtain the CNPs with optimized drug loading, the stoichiometric amount of cholesterol-drug conjugates **3**, **4**, and **6** were varied in different weight ratios. We observed a clear translation of the weight ratio into the final drug loading ratio with high drug loading efficiency in the CNPs with sub-200 nm size and comparable polydispersity index (PDI) values, determined by DLS (Table S1 in the Supporting Information). This ratiometric quantification clearly showed that the drug-loading ratio could be fine-tuned in the CNPs by using different stoichiometric amount of cholesterol-drug conjugates. However, we used PI103/doxoxrubicin/CDDP = 1:0.8:0.9 loading in CNPs for further studies having a mean drug loading of 252 μM, 204 μM, and 244 μM for PI103, doxorubicin, and cisplatin, respectively (Figure S14d in the Supporting Information). The mean size of the CNPs was found to be 153.7 nm in diameter by DLS (Figure 2a). Size, shape, and morphology of the CNPs were further visualized by FESEM (Figure 2b), AFM (Figure 2c), and TEM (Figure 2d). DLS and electron microscopy images clearly demonstrated that the CNPs were spherical in shape, at less than 200 nm in diameter, suitable for passive

DOI: 10.1021/acsami.5b04015
ACS Appl. Mater. Interfaces 2015, 7, 18327−18335

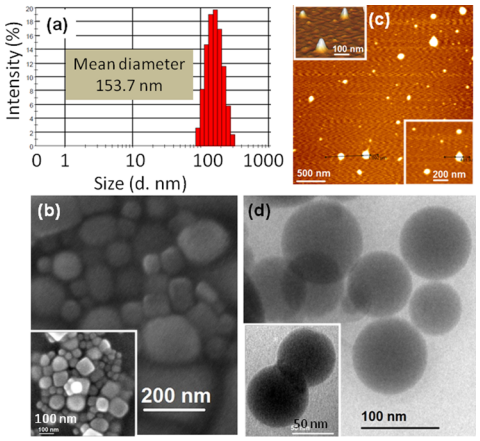

Figure 2. Characterization of size, shape, and morphology of CNPs by (a) DLS, (b) FESEM, (c) AFM, and (d) TEM.

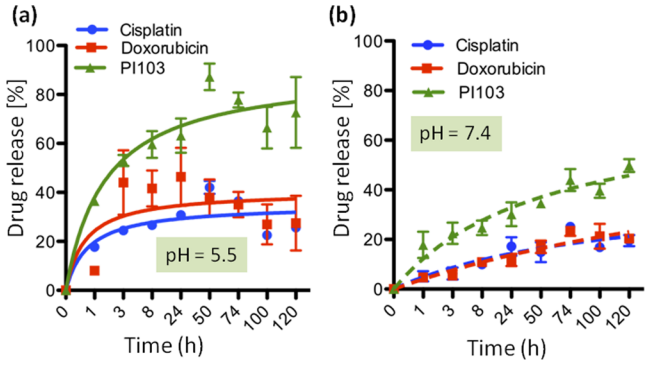

Figure 3. Release of PI103, doxorubicin, and cisplatin from CNPs at (a) pH = 5.5 and (b) pH = 7.4 over 120 h.

tumor targeting through leaky and tortuous vasculature. Furthermore, energy-dispersive X-ray spectroscopy (EDX) measurement was performed to demonstrate the presence of Pt metal from cisplatin in CNPs (Figure S15 in the Supporting Information).

3.3. Stability of the CNPs. To translate successfully from bench to bedside, the CNPs should maintain extensive stability over a long time under storage conditions. We estimated the stability of CNPs at 4 °C in PBS for 2 weeks by measuring size and PDI using DLS. Size of the CNPs changed marginally from 159.9 ± 2.9 nm (PDI = 0.105 ± 0.01) to 162.7 ± 1.4 nm (PDI = 0.132 ± 0.004) over 2 weeks (Figure S16a,b in the Supporting Information). Further, we measured the stability of the CNPs at 37 °C in PBS for 2 weeks. The size of the CNPs increased from 155.0 ± 1.7 nm with PDI = 0.069 ± 0.0 to 159.2 ± 1.3 nm with PDI = 0.81 ± 0.00) over 2 weeks (Figure S16c,d in the Supporting Information). For successful *in vivo* drug delivery, CNPs must show high stability inside the blood flow at body temperature. Therefore, we assessed the stability of CNPs in DMEM with 10% FBS at 37 °C for 72 h. The size of CNPs increased from 139.5 ± 0.4 nm to 154.6 ± 6.6 nm (change in PDI = 0.179 ± 0.0 to 0.214 ± 0.03) (Figure S16e,f in the Supporting Information). This stability measurements clearly showed that CNPs retained their size under 200 nm without major aggregation at 4 and 37 °C in PBS for 2 weeks as well as in the blood flow milieu for 72 h.

3.4. Release of Triple Drugs from CNPs. After accumulation inside the tumor, the CNPs must be able to release payloads in a controlled and continuous manner through a prolonged time. Moreover, the sequential administration of drugs in combination strategy plays a crucial role in the therapeutic outcome.[56,36] We anticipated that inhibiting PI3K signaling as a survival pathway followed by DNA damage would lead to better therapeutic efficacy. We quantified the release profile[43] of triple drugs from CNPs for 120 h at 37 °C in an acidic environment (pH = 5.5), which imitates the lysosomes in the cancer cells.[57] CNPs released 87.2 ± 5.3% of PI103 and 42.1 ± 2.6% of cisplatin at 50 h, whereas 46.4 ± 11.8% of doxorubicin was released at 24 h (Figure 3a). As a control, we evaluated the amount of triple drugs released from CNPs by incubating them at physiological pH = 7.4. CNPs released 49.7 ± 2.5% of PI103 after 120 h, whereas only 23.4 ± 1.9% of doxorubicin and 25.1 ± 0.8% cisplatin were released even after 74 h (Figure 3b). We further evaluated the presence of free PI103, doxorubicin, and cisplatin released from CNPs at pH = 5.5 after 24 and 48 h by UV−vis spectroscopy (Figure S17 in the Supporting Information). Figure S17a clearly showed the characteristic peaks at λ_{max} = 480 nm (for free doxorubicin) and 340 nm (for free PI103) in both 24 and 48 h time points (highlighted regions). Figure S17b also showed the characteristic peak at λ_{max} = 706 nm for free cisplatin in both 24 and 48 h (highlighted region). Finally, we confirmed the presence of free cisplatin, PI103, and doxorubicin released from CNPs at pH = 5.5 after 48 h incubation by MALDI-TOF (Figures S18 and S19 in the Supporting Information). From these UV−vis and MALDI-TOF data, it was clear that the structures of all the drugs retained after release from CNPs to show their pharmacological effects. These release data clearly showed that CNPs exhibited significantly increased drug release in a controlled and continuous manner over 120 h in an acidic environment compared to a neutral medium. We anticipated that ester, amide, and carboxylato-Pt bonds in the cholesterol-PI103 (**3**), cholesterol-doxorubicin (**4**) and cholesterol−cisplatin (**6**) conjugates respectively, are highly hydrolyzable in an acidic medium compared to a neutral medium, which prompted the superior triple drug release. Furthermore, at pH = 5.5, the aromatic ester bond in conjugate **3** is more hydrolyzable compared to the amide and carboxylato-Pt bond in conjugate **4** and conjugate **6**, respectively, which led to the faster and improved release of PI103 compared to doxorubicin and cisplatin. Finally, at pH = 5.5, we observed a decreased accumulative release for all the drugs after 50 h, which we attributed to the possible degradation of all the drugs in acidic condition after prolonged incubation.

3.5. *In Vitro* Cytotoxicity Assay of CNPs in Cancer Cells. To assess the effect of the CNPs in cancer therapy, we determined the *in vitro* efficacy of CNPs in HeLa cervical cancer cells, HL60 promyelocytic leukemia cells, and MCF7 metastatic breast cancer cells by MTT assay at 24 and 48 h post incubation. For the MTT assay, we used CNPs and free drug cocktails having the same PI103/doxorubicin/CDDP = 1:0.8:0.9 ratios. We also estimated the cytotoxicity of dual drug loaded CDDP-Dox-NPs, Dox-PI103-NPs, and CDDP-PI103-NPs as controls. At 24 h, CNPs showed much less IC_{50} = 4.1 μM compared to IC_{50} = 14.4 μM, 6.84 μM, 13.3 μM, and 6.58 μM for the free drug cocktail, CDDP-Dox-NPs, CDDP-PI103-NPs, and Dox-PI103-NPs, respectively, in HeLa cells (Figures S20a and S21a−c in the Supporting Information). Similarly, CNPs demonstrated IC_{50} = 1.5 μM compared to IC_{50} = 3 μM, 7.35 μM, 1.74 μM, and 0.41 μM for the free drug cocktail, CDDP-Dox-NPs, CDDP-PI103-NPs, and Dox-PI103-

DOI: 10.1021/acsami.5b04015
ACS Appl. Mater. Interfaces 2015, 7, 18327−18335

NPs, respectively, in HL60 cells at 24 h (Figures S20b and S22a–c in the Supporting Information). Moreover, CNPs showed IC_{50} = 14.9 μM compared to IC_{50} = 37.5 μM, 5.07 μM, 11.01 μM, and 7.17 μM for the free drug cocktail, CDDP-Dox-NPs, CDDP-PI103-NPs, and Dox-PI103-NPs, respectively, at 24 h in MCF7 cells (Figures S20c and S23a–c in the Supporting Information). At 48 h, CNPs showed IC_{50} = 0.87 μM which was equal to the IC_{50} = 0.86 μM for the free drug cocktail for HeLa cells (Figure 4a). However, at 48 h in HeLa cells, CDDP-Dox-NPs, CDDP-PI103-NPs, and Dox-PI103-NPs showed much higher IC_{50} = 4.89 μM, 3.33 μM, and 4.96 μM, respectively (Figure S21d–f in the Supporting Information). On the other hand, CNPs showed IC_{50} = 0.8 μM compared to IC_{50} = 1.9 μM, 0.79 μM, 0.07 μM, and 16.2 μM for free drug combination, CDDP-Dox-NPs, CDDP-PI103-NPs, and Dox-PI103-NPs, respectively, in HL60 cells at 48 h (Figure 4b and Figure S22d–f in the Supporting Information). Furthermore, at 48 h, CNPs showed IC_{50} = 3.2 μM compared to IC_{50} = 29.9 μM, 3.17 μM, 1.58 μM, and 0.39 μM for the free drug combination, CDDP-Dox-NPs, CDDP-PI103-NPs, and Dox-PI103-NPs, respectively, in MCF7 cells (Figure 4c and Figure S23d–f in the Supporting Information). We also evaluated the *in vitro* efficacy of CNPs in the triple negative breast cancer (TNBC) cell line MDA-MB-231 at 24 and 48 h post-treatment. Interestingly, CNPs showed extremely enhanced efficacy with IC_{50} = 0.4 μM compared to IC_{50} = 35.8 μM, 23.4 μM, 10.44 μM, and 24.24 μM for the free drug combination, CDDP-Dox-NPs, CDDP-PI103-NPs, and Dox-PI103-NPs, respectively, at 24 h (Figures S20d and S24a–c in the Supporting Information). At 48 h post-treatment, CNPs showed even more improved efficacy with IC_{50} = 0.2 μM compared to IC_{50} = 5.7 μM, 5.24 μM, 4.92 μM, and 3.20 μM for the free drug combinations, CDDP-Dox-NPs, CDDP-PI103-NPs, and Dox-PI103-NPs, respectively (Figure 4d and Figure S24d–f in the Supporting Information). These cell viability assays demonstrated that CNPs induced much better efficacy in HeLa and MDA-MB-231 cells with respect to free drug cocktails and dual drug loaded nanoparticles at 24 and 48 h. However, interestingly, in HL60 and MCF7 cells, CNPs showed much improved efficacy compared to the free drug combination but almost equivalent efficacy compared to dual drug loaded nanoparticles in both 24 and 48 h.

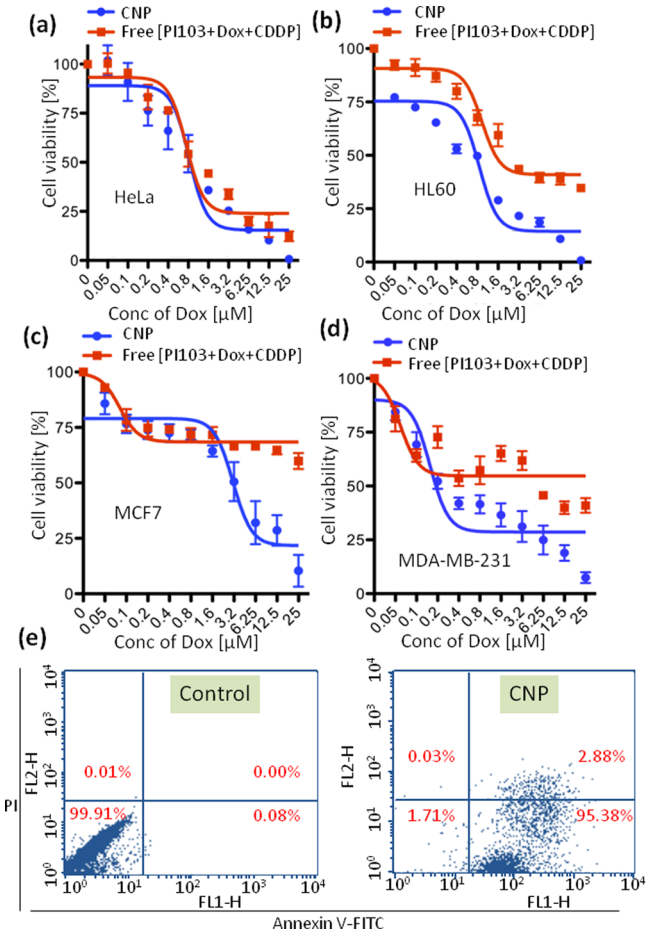

Figure 4. *In vitro* cytotoxicity assay of CNPs. (a–d) Cell viability assay of CNPs in HeLa, HL60, MCF7, and MDA-MB-231 cells for 48 h, respectively. (e) Fluorescence Assisted Cell Sorting (FACS) analysis of apoptosis caused by CNPs costained by Annexin V-FITC and PI in HeLa cells for 24 h. The values shown in each quadrant represents the percentage of cells present in healthy (lower left), early apoptotic (lower right), late apoptotic (upper right), and necrotic (upper left) states.

One of the hallmarks of cancer is its capability to evade apoptosis.[58] Hence, we evaluated the effect of CNPs in inducing apoptosis in cancer cells. We incubated HeLa cells with CNPs at IC_{50} values for 24 h, followed by staining the cell surface phosphatidylserine as an early apoptosis marker by green fluorescent Annexin V-FITC dye. We costained the cellular DNA of late apoptotic/necrotic cells with red fluorescent propidium iodide (PI). Quantification of early apoptotic, late apoptotic, and necrotic cells was performed using the fluorescence activated cell sorting (FACS) method. Indeed, CNPs induced early apoptosis in 95.38% cells and late apoptosis in 2.88% cells compared to only 0.08% and 0% cells found in the early and late apoptotic stages in the nontreated control cell (Figure 4e). This FACS analysis clearly demonstrated that CNPs showed antitumor activity by inducing apoptosis in HeLa cells.

3.6. Cellular Internalization of CNPs. To envision the temporal cellular internalization mechanism of CNPs, we incubated HeLa, MDA-MB-231, and MCF7 cells with red fluorescent CNPs (at 2 μg/mL concentration of doxorubicin) for 1, 3, and 6 h. The cells were fixed by paraformaldehyde, and acidic lysosomal compartments were stained by green fluorescent LysoTracker Green DND-26 dye. We also stained the nuclei with DAPI (blue) and visualized the cells by using CLSM. From Figure 5, it was clear that the CNPs entered into HeLa cells temporally over 6 h and localized into the lysosomes, leading to the colocalization of green and red merged into yellow. Quantification of the amount of localization of CNPs into the lysosomes from CLSM revealed that the percentage of colocalization was increased from 11.5% to 19.8% to 20.7% from 1 to 3 to 6 h, respectively, in HeLa cells (Table S2 in the Supporting Information). Figure 6 also clearly showed that the CNPs internalized into the MDA-MB-231 cells very rapidly within 6 h and localized into acidic lysosomal compartments in a time dependent manner. The CLSM based quantification of the % volume colocalization showed that 13.3%, 22.5%, and 52.2% CNPs were colocalized into lysosomes in 1 to 3 to 6 h, respectively (Table S3 in the Supporting Information). Furthermore, CLSM images also revealed that CNPs internalized and homed in the lysosomal compartments within 6 h in MCF7 cells (Figure S27 in the Supporting Information).

DOI: 10.1021/acsami.5b04015
ACS Appl. Mater. Interfaces 2015, 7, 18327–18335

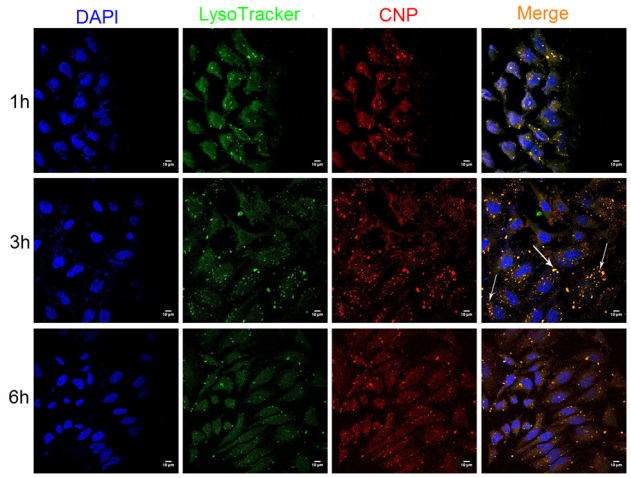

Figure 5. Internalization of CNPs in HeLa cells at 1, 3, and 6 h visualized by CLSM. Lysosomes and nuclei were stained by LysoTracker Green DND-26 and DAPI (blue), respectively. The merged images prove the homing (yellow) of CNPs in lysosomes. Scale = 10 μm.

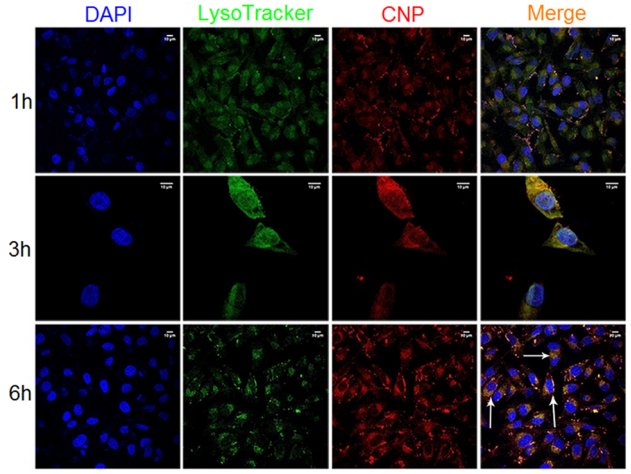

Figure 6. Internalization of CNPs in MDA-MB-231 cells at 1, 3, and 6 h visualized by CLSM. Lysosomes and nuclei were stained by LysoTracker Green DND-26 and DAPI (blue), respectively. The merged images illustrate the homing (yellow) of CNPs in lysosomes. Scale = 10 μm.

Lipidic nanoparticles have tendency to be exocytosed from the cells leading to the reduced efficacy in drug delivery.[59] To evaluate the existence of the CNPs into the cells for an extended period of time, we also evaluated the cellular internalization at 24 and 48 h time points in HeLa, MDA-MB-231, and MCF7 cells. Figures S25, S26, and S27 in the Supporting Information clearly demonstrated that CNPs were retained inside the acidic lysosomal compartments for 24 and 48 h to show their anticancer activity. CLSM based quantification revealed that 37.9% and 55.0% colocalization were observed for HeLa cells, compared to 37.7% and 27.9% colocalization observed for MDA-MB-231 cells (Tables S2 and S3 in the Supporting Information). We hypothesized that CNPs will be endocytosed into acidic lysosomal compartments, and in the acidic environment each drug will be released and inhibit their respective targets. From Figures S25, S26, and S27 in the Suppoting Information, it was clear that at 24 and 48 h, red fluorescent doxorubicin was localized into a blue fluorescent nucleus to afford a merged purple color in HeLa, MDA-MB-231, and MCF7 cells. We also quantified the colocalization of doxorubicin in the nucleus from CLSM. Tables S2 and S3 in the Supporting Information showed that the percentage of colocalization of blue and red colors gradually increased from 0.13% to 40.22% from 1 to 48 h in HeLa cells as well as from 7.28% to 48.5% from 1 to 48 h in MDA-MB-231 cells. These CLSM data demonstrated that the CNPs internalized into HeLa, MDA-MB-231, and MCF7 cells temporally by endocytosis followed by localization into the lysosomes for extended periods of time, leading to further release of triple drugs.

3.7. Mechanism of Action of CNPs. Phosphatidylinositol-3-kinase (PI3K) and its primary downstream mediator Akt play important roles in cell survival and proliferation in cancer cells.[60] As a result, PI3K-Akt signaling inhibitor PI103 showed improved efficacy in combination with doxorubicin as a DNA damaging agent.[17] Moreover, PI103 augmented the therapeutic efficacy of cisplatin nanoparticles in a breast cancer model.[42] However, there is no precedence of drug combination having PI103, doxorubicin, and cisplatin in a single nanoparticle. Hence, we evaluated the mechanism of action of CNPs in HeLa after treatment with CNPs at IC_{50} = 4.1 μM concentration for 24 h and visualized the protein expressions by Western blot. We evaluated the expression of γH2AX to monitor DNA damage.[61] Figure 7a demonstrated that CNPs induced

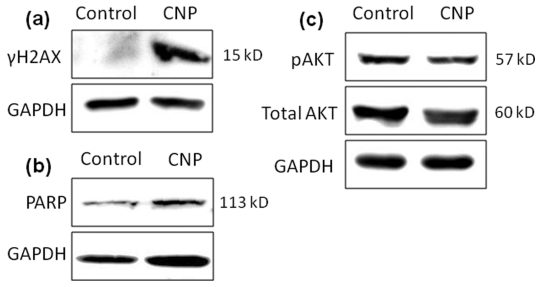

Figure 7. Expression of (a) γH2AX, (b) PARP, and (c) p-Akt in HeLa cells after 24 h post-incubation with CNPs determined by Western blot analysis.

significantly increased expression of γH2AX compared to no treatment. Quantification of the relative expression of γH2AX showed a 13-fold increase in CNP treated cells compared to no treatment, which clearly indicated that CNPs showed cytotoxicity by inducing DNA damage (Figure S28a in the Supporting Information).

After DNA damage, the poly(ADP-ribose) polymerase (PARP) family of proteins gets activated to repair the damage. As a result, PARP activation is also a potential biomarker for cellular DNA damage.[62] Evaluation of PARP expression (Figure 7b) showed that CNPs activated PARP compared to no treatment control. Furthermore, PARP quantification revealed a 3-fold increase upon incubation with CNPs relative to no treatment (Figure S28b in the Supporting Information).

Finally, we evaluated the expression of phospho-Akt, which is a downstream therapeutic target and one of the most important biomarkers in PI3K signaling. From Figure 7c, it was clear that CNPs reduced the expression of phosphor-Akt while keeping the total Akt expression the same compared to the no treatment control. Quantification from Western blot also showed a 1.4-fold decrease of phosphor-Akt expression upon treatment with CNPs compared to the control (Figure S28c in

DOI: 10.1021/acsami.5b04015
ACS Appl. Mater. Interfaces 2015, 7, 18327−18335

the Supporting Information). From these Western blot analyses, it was evident that CNPs demonstrated improved cytotoxicity in HeLa cells by inhibiting PI3K signaling and DNA damage.

4. CONCLUSION

We have engineered cholesterol-based chimeric nanoparticles (CNPs), which can simultaneously contain PI103, doxorubicin, and cisplatin in a controlled ratiometric manner. The CNPs released three drugs in a prolonged and continuous manner in enhanced quantity in an acidic medium compared to a neutral medium over 120 h with excellent stability at 4 and 37 °C over 2 weeks as well as in a blood circulation mimic for 72 h. The CNPs induced improved *in vitro* cytotoxicity against cervical cancer (HeLa), promyelocytic leukemia cells (HL60), and metastatic breast cancer cells (MCF7) as well as drug resistant triple negative breast cancer cells (MDA-MB-231) compared to the free drug combinations. These CNPs localized temporally into the acidic lysosomes after endocytosis within 6 h and were retained inside the cells for 48 h in HeLa, MDA-MB-231, and MCF7 cells. Finally, the CNPs showed their efficacy in HeLa cells by inhibiting PI3K-Akt signaling and inducing DNA damage, leading to the induction of apoptosis. We anticipate that these chimeric nanoparticles will open up a new avenue into rational multi-drug-combination therapy through targeting various critical oncogenic signaling pathways as well as delivering traditional chemotherapeutic drugs as personalized medicine to offer improved survival in cancer patients.

■ ASSOCIATED CONTENT

Supporting Information

The Supporting Information is available free of charge on the ACS Publications website at DOI: 10.1021/acsami.5b04015.

Structural characterization by NMR, UV−vis spectroscopy, EDX, stability evaluation, and in vitro biological characterization details (PDF)

■ AUTHOR INFORMATION

Corresponding Author

*E-mail: sudipta.basu@iiserpune.ac.in.

Author Contributions

†These authors contributed equally to this work.

Notes

The authors declare no competing financial interest.

■ ACKNOWLEDGMENTS

We are grateful to IISER-Pune for providing all of the instrumental facilities. S.B. also thanks DBT for the Ramalingaswami Fellowship (BT/RLF/Re-entry/13/2011) and SERB (SB/FT/CS-044/2012) for providing financial support. We also sincerely thank Dr. Shouvik Datta and the DST Nanoscience unit for providing FESEM and AFM facilities, respectively. We also thank Libi Anandi and Dr. Mayurika Lahiri for helping in Western blot experiments. We thank the DST Nanoscience unit for providing an AFM facility. Finally, S.P. is thankful to CSIR-UGC for a doctoral fellowship.

■ REFERENCES

(1) Ferlay, J.; Shin, H.-R.; Bray, F.; Forman, D.; Mathers, C.; Parkin, D. M. Estimates of Worldwide Burden of Cancer in 2008: GLOBOCAN 2008. *Int. J. Cancer* **2010**, *127*, 2893−2917.

(2) Siegel, R.; Ma, J.; Zou, Z.; Jemal, A. Cancer Statistics, 2014. *Ca-Cancer J. Clin.* **2014**, *64*, 9−29.

(3) Holohan, C.; Van Schaeybroeck, S.; Longley, D. B.; Johnston, P. G. Cancer Drug Resistance: An Evolving Paradigm. *Nat. Rev. Cancer* **2013**, *13*, 714−726.

(4) Longley, D. B.; Johnston, P. G. Molecular Mechanisms of Drug Resistance. *J. Pathol.* **2005**, *205*, 275−292.

(5) Engelman, J. A.; Luo, J.; Cantley, L. C. The Evolution of Phosphatidylinositol 3-Kinases as Regulators of Growth and Metabolism. *Nat. Rev. Genet.* **2006**, *7*, 606−619.

(6) Liu, P.; Cheng, H.; Roberts, T. M.; Zhao, J. J. Targeting the Phosphoinositide 3-Kinase Pathway in Cancer. *Nat. Rev. Drug Discovery* **2009**, *8*, 627−644.

(7) Vanhaesebroeck, B.; Guillermet-Guibert, J.; Graupera, M.; Bilanges, B. The Emerging Mechanisms of Isoform-Specific PI3K Signalling. *Nat. Rev. Mol. Cell Biol.* **2010**, *11*, 329−341.

(8) Workman, P.; Clarke, P. A.; Raynaud, F. I.; Van Montfort, R. L. M. Drugging the PI3 Kinome: From Chemical Tools to Drugs in the Clinic. *Cancer Res.* **2010**, *70*, 2146−2157.

(9) Rückle, T.; Schwarz, M. K.; Rommel, C. PI3Kgamma Inhibition: Towards an "Aspirin of the 21st Century"? *Nat. Rev. Drug Discovery* **2006**, *5*, 903−918.

(10) Hennessy, B. T.; Smith, D. L.; Ram, P. T.; Lu, Y.; Mills, G. B. Exploiting the PI3K/AKT Pathway for Cancer Drug Discovery. *Nat. Rev. Drug Discovery* **2005**, *4*, 988−1004.

(11) Cho, H.; Mu, J.; Kim, J. K.; Thorvaldsen, J. L.; Chu, Q.; Crenshaw, E. B.; Kaestner, K. H.; Bartolomei, M. S.; Shulman, G. I.; Birnbaum, M. J. Insulin Resistance and a Diabetes Mellitus-Like Syndrome in Mice Lacking the Protein Kinase Akt2 (PKB Beta). *Science* **2001**, *292*, 1728−1731.

(12) Taniguchi, C. M.; Tran, T. T.; Kondo, T.; Luo, J.; Ueki, K.; Cantley, L. C.; Kahn, C. R. Phosphoinositide 3-Kinase Regulatory Subunit P85α Suppresses Insulin Action via Positive Regulation of PTEN. *Proc. Natl. Acad. Sci. U. S. A.* **2006**, *103*, 12093−12097.

(13) Knight, Z. A.; Gonzalez, B.; Feldman, M. E.; Zunder, E. R.; Goldenberg, D. D.; Williams, O.; Loewith, R.; Stokoe, D.; Balla, A.; Toth, B.; Balla, T.; Weiss, W. A.; Williams, R. L.; Shokat, K. M. A Pharmacological Map of the PI3-K Family Defines a Role for p110α in Insulin Signaling. *Cell* **2006**, *125*, 733−747.

(14) Bendell, J. C.; Rodon, J.; Burris, H. a; de Jonge, M.; Verweij, J.; Birle, D.; Demanse, D.; De Buck, S. S.; Ru, Q. C.; Peters, M.; Goldbrunner, M.; Baselga, J. Phase I, Dose-Escalation Study of BKM120, An Oral Pan-Class I PI3K Inhibitor, in Patients with Advanced Solid Tumors. *J. Clin. Oncol.* **2012**, *30*, 282−290.

(15) Opel, D.; Westhoff, M. A.; Bender, A.; Braun, V.; Debatin, K. M.; Fulda, S. Phosphatidylinositol 3-Kinase Inhibition Broadly Sensitizes Glioblastoma Cells to Death Receptor- and Drug-Induced Apoptosis. *Cancer Res.* **2008**, *68*, 6271−6280.

(16) Westhoff, M.-A.; Kandenwein, J. A.; Karl, S.; Vellanki, S. H. K.; Braun, V.; Eramo, A.; Antoniadis, G.; Debatin, K.-M.; Fulda, S. The Pyridinylfuranopyrimidine Inhibitor, PI-103, Chemosensitizes Glioblastoma Cells for Apoptosis by Inhibiting DNA Repair. *Oncogene* **2009**, *28*, 3586−3596.

(17) Marklein, D.; Graab, U.; Naumann, I.; Yan, T.; Ridzewski, R.; Nitzki, F.; Rosenberger, A.; Dittmann, K.; Wienands, J.; Wojnowski, L.; Fulda, S.; Hahn, H. PI3K Inhibition Enhances Doxorubicin-Induced Apoptosis in Sarcoma Cells. *PLoS One* **2012**, *7*, e52898.

(18) Peer, D.; Karp, J. M.; Hong, S.; Farokhzad, O. C.; Margalit, R.; Langer, R. Nanocarriers as An Emerging Platform for Cancer Therapy. *Nat. Nanotechnol.* **2007**, *2*, 751−760.

(19) Kim, B. Y. S.; Rutka, J. T.; Chan, W. C. W. Nanomedicine. *N. Engl. J. Med.* **2010**, *363*, 2434−2443.

(20) Ediriwickrema, A.; Saltzman, W. M. Nanotherapy for Cancer: Targeting and Multifunctionality in The Future of Cancer Therapies. *ACS Biomater. Sci. Eng.* **2015**, *1*, 64−78.

(21) Cheng, C. J.; Tietjen, G. T.; Saucier-Sawyer, J. K.; Saltzman, W. M. A Holistic Approach to Targeting Disease with Polymeric Nanoparticles. *Nat. Rev. Drug Discovery* **2015**, *14*, 239−247.

(22) Couvreur, P.; Vauthier, C. Nanotechnology: Intelligent Design to Treat Complex Disease. *Pharm. Res.* **2006**, *23*, 1417−1450.
(23) Yuan, F.; Dellian, M.; Fukumura, D.; Leunig, M.; Berk, D. A.; Torchilin, V. P.; Jain, R. K. Vascular Permeability in a Human Tumor Xenograft: Molecular Size Dependence and Cutoff Size. *Cancer Res.* **1995**, *55*, 3752−3756.
(24) Hobbs, S. K.; Monsky, W. L.; Yuan, F.; Roberts, W. G.; Griffith, L.; Torchilin, V. P.; Jain, R. K. Regulation of Transport Pathways in Tumor Vessels: Role of Tumor Type and Microenvironment. *Proc. Natl. Acad. Sci. U. S. A.* **1998**, *95*, 4607−4612.
(25) Torchilin, V. P. Recent Advances with Liposomes as Pharmaceutical Carriers. *Nat. Rev. Drug Discovery* **2005**, *4*, 145−160.
(26) Morton, S. W.; Lee, M. J.; Deng, Z. J.; Dreaden, E. C.; Siouve, E.; Shopsowitz, K. E.; Shah, N. J.; Yaffe, M. B.; Hammond, P. T. A Nanoparticle-Based Combination Chemotherapy Delivery System for Enhanced Tumor Killing by Dynamic Rewiring of Signaling Pathways. *Sci. Signaling* **2014**, *7*, ra44.
(27) Kolishetti, N.; Dhar, S.; Valencia, P. M.; Lin, L. Q.; Karnik, R.; Lippard, S. J.; Langer, R.; Farokhzad, O. C. Engineering of Self-Assembled Nanoparticle Platform for Precisely Controlled Combination Drug Therapy. *Proc. Natl. Acad. Sci. U. S. A.* **2010**, *107*, 17939−17944.
(28) Wang, H.; Zhao, Y.; Wu, Y.; Hu, Y.; Nan, K.; Nie, G.; Chen, H. Enhanced Anti-Tumor Efficacy by Co-Delivery of Doxorubicin and Paclitaxel with Amphiphilic Methoxy PEG-PLGA Copolymer Nanoparticles. *Biomaterials* **2011**, *32*, 8281−8290.
(29) Liao, L.; Liu, J.; Dreaden, E. C.; Morton, S. W.; Shopsowitz, K. E.; Hammond, P. T.; Johnson, J. A. A Convergent Synthetic Platform for Single-Nanoparticle Combination Cancer Therapy: Ratiometric Loading and Controlled Release of Cisplatin, Doxorubicin, and Camptothecin. *J. Am. Chem. Soc.* **2014**, *136*, 5896−5899.
(30) Kaneshiro, T. L.; Lu, Z. R. Targeted Intracellular Codelivery of Chemotherapeutics and Nucleic Acid with A Well-Defined Dendrimer-Based Nanoglobular Carrier. *Biomaterials* **2009**, *30*, 5660−5666.
(31) Han, L.; Huang, R.; Li, J.; Liu, S.; Huang, S.; Jiang, C. Plasmid Porf-Htrail and Doxorubicin Co-Delivery Targeting to Tumor using Peptide-Conjugated Polyamidoamine Dendrimer. *Biomaterials* **2011**, *32*, 1242−1252.
(32) Zhang, L.; Xia, J.; Zhao, Q.; Liu, L.; Zhang, Z. Functional Graphene Oxide as a Nanocarrier for Controlled Loading and Targeted Delivery of Mixed Anticancer Drugs. *Small* **2010**, *6*, 537−544.
(33) Zhang, L.; Lu, Z.; Zhao, Q.; Huang, J.; Shen, H.; Zhang, Z. Enhanced Chemotherapy Efficacy by Sequential Delivery of siRNA and Anticancer Drugs Using PEI-Grafted Graphene Oxide. *Small* **2011**, *7*, 460−464.
(34) Chin, C. F.; Yap, S. Q.; Li, J.; Pastorin, G.; Ang, W. H. Ratiometric Delivery of Cisplatin and Doxorubicin using Tumour-Targeting Carbon-Nanotubes Entrapping Platinum(IV) Prodrugs. *Chem. Sci.* **2014**, *5*, 2265−2270.
(35) Fang, Y.; Zheng, G.; Yang, J.; Tang, H.; Zhang, Y.; Kong, B.; Lv, Y.; Xu, C.; Asiri, A. M.; Zi, J.; Zhang, F.; Zhao, D. Dual-Pore Mesoporous Carbon@Silica Composite Core−Shell Nanospheres for Multidrug Delivery. *Angew. Chem., Int. Ed.* **2014**, *53*, 5366−5370.
(36) Sengupta, S.; Eavarone, D.; Capila, I.; Zhao, G.; Watson, N.; Kiziltepe, T.; Sasisekharan, R. Novel Cancer Therapy Through Temporal Targeting of Both Tumor Cells and Neovasculature Using a Unique Nanoscale Delivery System. *Nature* **2005**, *436*, 568−572.
(37) Jiang, T.; Mo, R.; Bellotti, A.; Zhou, J.; Gu, Z. Gel−Liposome-Mediated Co-Delivery of Anticancer Membrane-Associated Proteins and Small-Molecule Drugs for Enhanced Therapeutic Efficacy. *Adv. Funct. Mater.* **2014**, *24*, 2295−2304.
(38) Deng, Z. J.; Morton, S. W.; Ben-Akiva, E.; Dreaden, E. C.; Shopsowitz, K. E.; Hammond, P. T. Layer-by-Layer Nanoparticles for Systemic Codelivery of An Anticancer Drug and Sirna for Potential Triple-Negative Breast Cancer Treatment. *ACS Nano* **2013**, *7*, 9571−9584.
(39) MacDiarmid, J. A.; Amaro-Mugridge, N. B.; Madrid-Weiss, J.; Sedliarou, I.; Wetzel, S.; Kochar, K.; Brahmbhatt, V. N.; Phillips, L.; Pattison, S. T.; Petti, C.; Stillman, B.; Graham, R. M.; Brahmbhatt, H. Sequential Treatment of Drug-Resistant Tumors with Targeted Minicells Containing SiRNA or A Cytotoxic Drug. *Nat. Biotechnol.* **2009**, *27*, 643−651.
(40) Harfouche, R.; Basu, S.; Soni, S.; Hentschel, D.; Mashelkar, R.; Sengupta, S. Nanoparticle-Mediated Targeting of Phosphatidylinositol-3-Kinase Signaling Inhibits Angiogenesis. *Angiogenesis* **2009**, *12*, 325−338.
(41) Kulkarni, A. A.; Roy, B.; Rao, P. S.; Wyant, G. A.; Mahmoud, A.; Ramachandran, M.; Sengupta, P.; Goldman, A.; Kotamraju, V. R.; Basu, S.; Mashelkar, R. A.; Ruoslahti, E.; Dinulescu, D. M.; Sengupta, S. Supramolecular Nanoparticles that Target Phosphoinositide-3-Kinase Overcome Insulin Resistance and Exert Pronounced Antitumor Efficacy. *Cancer Res.* **2013**, *73*, 6987−6997.
(42) Pandey, A.; Kulkarni, A.; Roy, B.; Goldman, A.; Sarangi, S.; Sengupta, P.; Phipps, C.; Kopparam, J.; Oh, M.; Basu, S.; Kohandel, M.; Sengupta, S. Sequential Application of A Cytotoxic Nanoparticle and A PI3K Inhibitor Enhances Antitumor Efficacy. *Cancer Res.* **2014**, *74*, 675−685.
(43) Sengupta, P.; Basu, S.; Soni, S.; Pandey, A.; Roy, B.; Oh, M. S.; Chin, K. T.; Paraskar, A. S.; Sarangi, S.; Connor, Y.; Sabbisetti, V. S.; Kopparam, J.; Kulkarni, A.; Muto, K.; Amarasiriwardena, C.; Jayawardene, I.; Lupoli, N.; Dinulescu, D. M.; Bonventre, J. V.; Mashelkar, R. A.; Sengupta, S. Cholesterol-Tethered Platinum II-Based Supramolecular Nanoparticle Increases Antitumor Efficacy and Reduces Nephrotoxicity. *Proc. Natl. Acad. Sci. U. S. A.* **2012**, *109*, 11294−11299.
(44) Mallick, A.; More, P.; Ghosh, S.; Chippalkatti, R.; Chopade, B. A.; Lahiri, M.; Basu, S. Dual Drug Conjugated Nanoparticle for Simultaneous Targeting of Mitochondria and Nucleus in Cancer Cells. *ACS Appl. Mater. Interfaces* **2015**, *7*, 7584−7598.
(45) Palvai, S.; Nagraj, J.; Mapara, N.; Chowdhury, R.; Basu, S. Dual Drug Loaded Vitamin D3 Nanoparticle to Target Drug Resistance in Cancer. *RSC Adv.* **2014**, *4*, 57271−57281.
(46) Voet, D.; Voet, J. *Biochemistry*, 3rd ed; John Wiley & Sons, Inc: New York, 2012; pp 765−796.
(47) Fan, Q. W.; Knight, Z. A.; Goldenberg, D. D.; Yu, W.; Mostov, K. E.; Stokoe, D.; Shokat, K. M.; Weiss, W. A. A Dual PI3 Kinase/MTOR Inhibitor Reveals Emergent Efficacy in Glioma. *Cancer Cell* **2006**, *9*, 341−349.
(48) Aronov, O.; Horowitz, A. T.; Gabizon, A.; Gibson, D. Folate-Targeted PEG as A Potential Carrier for Carboplatin Analogs. Synthesis and In Vitro Studies. *Bioconjugate Chem.* **2003**, *14*, 563−574.
(49) Brown, S. D.; Nativo, P.; Smith, J. A.; Stirling, D.; Edwards, P. R.; Venugopal, B.; Flint, D. J.; Plumb, J. A.; Graham, D.; Wheate, N. J. Gold Nanoparticles for the Improved Anticancer Drug Delivery of The Active Component of Oxaliplatin. *J. Am. Chem. Soc.* **2010**, *132*, 4678−4684.
(50) Still, B. M.; Kumar, P. G. A.; Aldrich-Wright, J. R.; Price, W. S. 195Pt NMR–Theory and Application. *Chem. Soc. Rev.* **2007**, *36*, 665−686.
(51) Sengupta, P.; Basu, S.; Soni, S.; Pandey, A.; Roy, B.; Oh, M. S.; Chin, K. T.; Paraskar, A. S.; Sarangi, S.; Connor, Y.; Sabbisetti, V. S.; Kopparam, J.; Kulkarni, A.; Muto, K.; Amarasiriwardena, C.; Jayawardene, I.; Lupoli, N.; Dinulescu, D. M.; Bonventre, J. V.; Mashelkar, R. A.; Sengupta, S. Cholesterol-Tethered Platinum II-Based Supramolecular Nanoparticle Increases Antitumor Efficacy and Reduces Nephrotoxicity. *Proc. Natl. Acad. Sci. U. S. A.* **2012**, *109*, 11294−11299.
(52) Harris, J. M.; Chess, R. B. Effect of Pegylation on Pharmaceuticals. *Nat. Rev. Drug Discovery* **2003**, *2*, 214−221.
(53) Raynaud, F. I.; Eccles, S. A.; Patel, S.; Alix, S.; Box, G.; Chuckowree, I.; Folkes, A.; Gowan, S.; De Haven Brandon, A.; Di Stefano, F.; Hayes, A.; Henley, A. T.; Lensun, L.; Pergl-Wilson, G.; Robson, A.; Saghir, N.; Zhyvoloup, A.; McDonald, E.; Sheldrake, P.; Shuttleworth, S.; Valenti, M.; Wan, N. C.; Clarke, P. A.; Workman, P. Biological Properties of Potent Inhibitors of Class I Phosphatidylinosi-

DOI: 10.1021/acsami.5b04015
ACS Appl. Mater. Interfaces 2015, 7, 18327−18335

tide 3-Kinases: From PI-103 Through PI-540, PI-620 to The Oral Agent GDC-0941. *Mol. Cancer Ther.* **2009**, *8*, 1725−1738.
(54) Minotti, G.; Menna, P.; Salvatorelli, E.; Cairo, G.; Gianni, L. Anthracyclines: Molecular Advances and Pharmacologic Developments in Antitumor Activity and Cardiotoxicity. *Pharmacol. Rev.* **2004**, *56*, 185−229.
(55) Yao, X.; Panichpisal, K.; Kurtzman, N.; Nugent, K. Cisplatin Nephrotoxicity: A Review. *Am. J. Med. Sci.* **2007**, *334*, 115−124.
(56) Lee, M. J.; Ye, A. S.; Gardino, A. K.; Heijink, A. M.; Sorger, P. K.; MacBeath, G.; Yaffe, M. B. Sequential Application of Anticancer Drugs Enhances Cell Death by Rewiring Apoptotic Signaling Networks. *Cell* **2012**, *149*, 780−794.
(57) Gilleron, J.; Querbes, W.; Zeigerer, A.; Borodovsky, A.; Marsico, G.; Schubert, U.; Manygoats, K.; Seifert, S.; Andree, C.; Stöter, M.; Epstein-Barash, H.; Zhang, L.; Koteliansky, V.; Fitzgerald, K.; Fava, E.; Bickle, M.; Kalaidzidis, Y.; Akinc, A.; Maier, M.; Zerial, M. Image-Based Analysis of Lipid Nanoparticle-Mediated siRNA Delivery, Intracellular Trafficking and Endosomal Escape. *Nat. Biotechnol.* **2013**, *31*, 638−646.
(58) Hanahan, D.; Weinberg, R. A. The Hallmarks of Cancer. *Cell* **2000**, *100*, 57−70.
(59) Sahay, G.; Querbes, W.; Alabi, C.; Eltoukhy, A.; Sarkar, S.; Zurenko, C.; Karagiannis, E.; Love, K.; Chen, D.; Zoncu, R.; Buganim, Y.; Schroeder, A.; Langer, R.; Anderson, D. G. Efficiency of siRNA Delivery by Lipid Nanoparticles Is Limited by Endocytic Recycling. *Nat. Biotechnol.* **2013**, *31*, 653−658.
(60) Franke, T. F. PI3K/Akt: Getting it Right Matters. *Oncogene* **2008**, *27*, 6473−6488.
(61) Kuo, L. J.; Yang, L.-X. Gamma-H2AX - A Novel Biomarker for DNA Double-Strand Breaks. *In Vivo* **2008**, *22*, 305−309.
(62) Curtin, N. J. DNA Repair Dysregulation From Cancer Driver to Therapeutic Target. *Nat. Rev. Cancer* **2012**, *12*, 801−817.

DOI: 10.1021/acsami.5b04015
ACS Appl. Mater. Interfaces 2015, 7, 18327−18335